Progress In Electromagnetics Research, Vol. 125, 503–526, 2012

ELECTROMAGNETIC AND THERMAL ANALYSES OF IMPROVED GTEM CELLS FOR BIOELECTROMAGNETIC EXPERIMENTS

G. Calò* and V. Petruzzelli

Dipartimento di Elettrotecnica ed Elettronica, Politecnico di Bari, Via Re David n. 200, Bari 70125, Italy

Abstract—A GHz Transverse Electromagnetic (GTEM) cell is proposed to investigate the arising of biological effects due to electromagnetic signals at the typical frequencies of mobile phone communications. The proposed GTEM cell, placed within a commercial incubator, has been ad hoc designed and fabricated to expose in vitro samples. The electromagnetic and the thermal analyses of the GTEM cell are reported. In particular, the inner electromagnetic field and the Specific Absorption Rate of the exposed sample (saline solution having 9 g/l concentration) have been evaluated by a home-made computer code based on the transmission line matrix method. Furthermore, the thermal analysis of the exposure arrangement has been carried out by the finite difference time domain algorithm.

1. INTRODUCTION

In recent years, many studies have been devoted to the investigation of radiofrequency (RF) and microwave (MW) radiations as promoters of possible adverse and dangerous effects on human health. A challenging goal is the assessment of a complete and exhaustive knowledge of the bioelectromagnetic interaction mechanisms that underlie such effects both at macroscopic and at microscopic levels. For this purpose, in vivo and in vitro experiments can give complementary information on the interaction between electromagnetic (e.m.) field sources and living organisms. On one hand, owing to the complexity of the reaction to external stimuli and stresses, in vivo experiments are useful to provide a realistic representation of the environmental radiation conditions for

Received 22 December 2011, Accepted 23 January 2012, Scheduled 7 March 2012

* Corresponding author: Giovanna Calo (g.calo@deemail.poliba.it).

living organisms. On the other hand, in vitro studies can provide precious information on the molecular and cellular changes induced by the e.m. fields thus helping to understand how the e.m. waves can cause a biological effect within the human body.

The choice of the test environment is crucial to bioelectromagnetic interaction experiments since reliability, repeatability and reproducibility of the measurements are strictly required. For this aim, different exposure systems have been proposed for in vitro [1–4] and in vivo [5–7] dosimetric experiments exploiting different electromagnetic devices (e.g., resonant waveguides, Wire Patch Cells (WPC), Transverse Electromagnetic (TEM) cells) and also GHz Transverse Electromagnetic (GTEM) cells [8–10]. Further insight in the bioelectromagnetic problem is given by numerical models which analyze the whole body dosimetry [11–13], the electromagnetic and thermal effects of the irradiation of specific organs (e.g., the human eye or the brain) [14, 15], the electromagnetic interaction at the cell membrane level [16] or the Specific Absorption Rate (SAR) distribution of in vitro cell cultures [17].

Considering the in vitro exposure systems proposed in the literature, a general classification can divide them into two categories: resonant and travelling wave devices. For example, the resonant waveguides and the WPCs belong to the first category. In particular, the resonant waveguide setup [2] is made of a rectangular waveguide terminated with reflecting walls so that the biological samples are placed inside the maxima of the resonant electromagnetic mode. The WPC, instead, is basically a parallel plate resonator, excited by a central feed, in which large electric field values are achieved between the plates [3]. Both resonant systems proved effective in assessing high SAR values, but their bandwidth is intrinsically narrow, it being limited by the resonant condition which occurs at discrete frequencies. Therefore, these systems offer limited flexibility in the exposure protocols since a change in the frequency of the experiment requires a new design of the exposure system. This limitation can be overcame by travelling wave devices such as the TEM and the GTEM cells which can operate in a broadband range.

The TEM cell consists of a rectangular coaxial transmission line tapered at both ends to be connected with standard 50-Ω coaxial cable. The GTEM cell is a rectangular coaxial transmission line tapered along the propagation direction and terminated on a broadband load. The TEM mode propagating in both the TEM and GTEM cells simulates a free-space plane-wave irradiation. The main difference between the two TEM systems is given by the upper frequency limit which is in the order of hundreds of MHz for the TEM cell, whereas it reaches a few GHz in the case of the GTEM cell. The TEM cell frequency

limit is determined by the appearance of higher-order modes, which resonate in the TEM cell, thus perturbing the desired TEM mode field distribution. Conversely, in the GTEM cell, the broadband matched load acts to suppress the creation of higher-order modes and to avoid undesired resonances.

In the context of dosimetric experiments, resonant structures should be preferred when high SAR values are required in narrow bandwidths, such as about 1–2 MHz [2] around the central resonant frequency. Conversely, TEM and GTEM cells are advantageous with respect to resonant structures, when a broadband operation is required for the investigation of biological effects of the electromagnetic field over different frequency ranges.

Here, we propose a new version of the GTEM cell specifically designed for the investigation of bioelectromagnetic interaction in the frequency range of Global System for Mobile Communications (GSM) and wireless systems. Conventional GTEM cells are commonly exploited to perform electromagnetic conformity tests on electric and electronic apparatuses [18] in a restricted and shielded enclosure. The novelty of the proposed system is mainly linked to its reduced sizes (0.45-m maximum length) as compared to the conventional GTEM cells, the sizes of which are generally several meters long.

Furthermore, the proposed exposure system allows a controlled TEM mode irradiation to assure the experiment repeatability, it guarantees a large test volume with respect to the whole volume and it assures a wide frequency range irradiation (up to a few GHz). The proposed GTEM cell allows to achieve different exposure conditions in terms of e.m. field frequency and amplitude, exposure time and SAR, i.e., the amount of electromagnetic power absorbed by the exposed biological sample. Moreover, the optimal thermodynamic conditions, an essential prerequisite for the survival of the biological sample, are guaranteed by the insertion of the GTEM cell into an incubator. Thanks to its portability and to its e.m. features, this device can be a valid aid to every research laboratory involved in bioelectromagnetic researches.

This paper deals with the main characteristics of the designed and fabricated GTEM-cell exposure system, particularly detailing the numerical analysis and the experimental characterization of the proposed dosimetric setup. More insights are given into the e.m. and thermal simulations of the dosimetric setup performed by homemade computer codes based on the Transmission Line Matrix (TLM) method and on the Finite Difference Time Domain (FDTD) algorithm, respectively [19–22]. Furthermore, the simulation results are compared with those obtained by temperature measurements.

2. GTEM CELL PROTOTYPE AND EXPOSURE SETUP

Figure 1 shows the photo of the first GTEM cell prototype enclosed in the incubator. It is a tapered TEM waveguide made of aluminum. The internal conductor, hereafter referred to as septum, is made of a Printed Circuit Board (PCB) suitably shaped to maintain the optimal aspect ratio that assures a 50-Ω characteristic impedance along the propagation direction. The low-frequency impedance matching was achieved by a 50-Ω resistive network load inserted in the PCB to connect the septum to the GTEM cell terminal wall. Owing to the reduced sizes of the proposed GTEM cell as compared with the several-meter-long conventional ones, the impedance matching in the frequency range of GSM and wireless communications required suitable configurations of absorbing loads to be chosen in the different frequency intervals, i.e., 1) ferrite tiles together with graphite absorbers, homemade by enriching dielectric foam with graphite powder to be used for frequencies around $f = 0.9\,\mathrm{GHz}$ and 2) a combination of short 7-cm pyramidal dielectric absorbers and ferrite tiles to be used for frequencies up to 3 GHz. For the two load configurations a Standing Wave Ratio (SWR) below 1.5 was measured in the investigated frequency ranges. Further details on the e.m. characterization of the proposed GTEM cell are given in [1, 23].

The insertion of the exposure systems in the incubator guarantees the optimal thermodynamic conditions indispensable for the survival of the exposed biological samples.

In particular, stable temperature ($37\,^{\circ}\mathrm{C} \pm 0.1^{\circ}\mathrm{C}$), humidified environment and controlled CO_2 level (5%) are required. For this purpose, a large number of ventilation holes were made on the GTEM

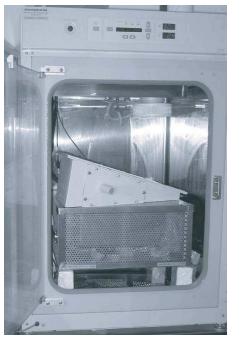

Figure 1. Photo of the GTEM cell prototype enclosed in the incubator.

cell walls allowing the air to flow from the incubator to the inner volume of the GTEM cell. In addition, as shown in Fig. 1, a cut-off waveguide aperture on the GTEM cell side door was made for the insertion of control probes during the exposure. The small size of these apertures with respect to the wavelength preserves the shielding effectiveness necessary to guarantee the electromagnetic compatibility with external instrumentation and the operator safety.

Although optimized, the thermodynamic conditions within the GTEM cell can still slightly differ from those pertaining to the incubator. Consequently, sham exposure (i.e., equivalent biological samples are contemporarily inserted in two equal GTEM cells with and without e.m. irradiation, respectively) must be taken into account. This standard practice allows to correctly evaluate whether a biological response is specifically ascribable to the e.m. irradiation or to the mere insertion of the cell cultures in the GTEM cell (regardless from the e.m. irradiation).

A scheme of the overall dosimetric setup is shown in Fig. 2. Here, two GTEM cell replicas are inserted into the incubator and are connected, through a switch and a directional coupler, to a signal generator and to an amplifier. The switch allows to randomly select which of the two GTEM cells irradiates the biological sample. Furthermore, the dosimetric experiment is remotely controlled by an ad-hoc developed software devoted to fix the exposure conditions (e.g., input signal frequency, input power, sham exposure, etc.) and to control the relevant dosimetric parameters (i.e., temperature, incident and reflected power, etc.). For this purpose, a power meter, connected to the GTEM cells through a directional coupler, monitors the incident and the reflected powers, whereas optical fiber probes continuously record the temperature variation within the biological samples.

To assess the desired exposure conditions during the dosimetric experiments, the SAR of the irradiated biological sample must be carefully evaluated. For this aim, as it will be described in the next sections, the electromagnetic and the thermodynamic behavior of the GTEM cell with the inserted biological sample will be analyzed.

3. ELECTROMAGNETIC ANALYSIS OF THE GTEM CELL

The e.m. simulations of the GTEM cell were performed by means of a homemade computing code based on the Transmission Line Matrix (TLM) method [19–21]. The TLM method allows a time domain solution of the Maxwell equations, modeling the e.m. propagation by means of a transmission line network. The simulation domain is

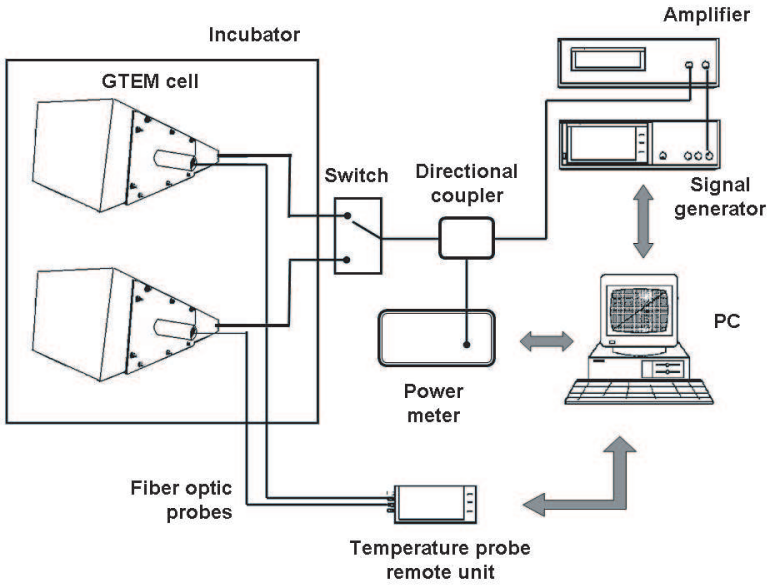

Figure 2. Scheme of the GTEM cell dosimetric setup.

partitioned in elementary subvolumes, referred to as Hybrid Symmetric Condensed Node (HSCN), each associated with a multiple-port elementary network made of uncoupled transmission lines. Thanks to the analogy between the Maxwell equations and the transmission line equations, the TLM algorithm allows to derive the e.m. field components from the knowledge of the voltage and current at each transmission line port. The solution of the Maxwell equations is, therefore, obtained by discretizing both space and time and by calculating the voltage and current waves at each transmission line composing the HSCN node.

Figure 3 illustrates two sections of the GTEM cell and a cylindrical biological sample. In the numerical model, the Cartesian axis system is centered in the apex of the pyramidal shape of the GTEM cell and the z axis corresponds to the propagation direction of the TEM wave. The HSCN grid gives a staircase approximation of the GTEM cell tapered shape and of the cylindrical shape of the sample (having diameter $d_s = 0.040\,\mathrm{m}$ and height $h_s = 0.020\,\mathrm{m}$). The sample distance D from the GTEM cell apex, the rise distance H from the lower GTEM cell wall, and the local axis system (x', y', z') centered within the sample are shown in Fig. 3, too.

The time domain simulations of the e.m. field components were

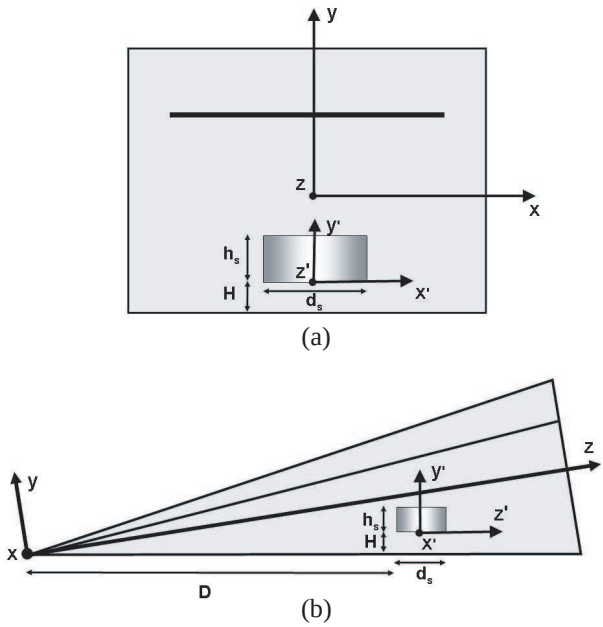

Figure 3. Sections of the GTEM cell with an included cylindrical biological sample. (a) x-y cross-section. (b) y-z cross-section.

performed by virtue of a uniform spatial grid made of HSCN nodes having size $\Delta l = 0.002\,\text{m}$. To achieve the numerical convergence, a time step $\Delta t = 3.3\,\text{ps}$ was chosen to fulfill the convergence criterion

$$\Delta t = \frac{\Delta l}{2\,\nu}$$

that links the time step Δt to the smallest space step Δl by the light velocity ν in the medium. The e.m. analysis in the three-dimensional model of the GTEM cell makes use of a sinusoidal voltage signal impressed at the HSCN nodes of section $z = 0.030\,\text{m}$. Specifically, a signal frequency $f = 1.8\,\text{GHz}$ has been chosen.

As a part of the validation of the TLM algorithm, the calculated e.m. field components were compared with the ones obtained by the Transverse Resonance Diffraction (TRD) [23, 24]. The TRD method allows a rigorous e.m. analysis of the GTEM cell by an analytical evaluation of the e.m. field components pertaining to the fundamental TEM wave and to the higher order modes. Although substantially different, the aforementioned methods showed a good agreement since a maximum 2% deviation was calculated by comparing the TLM and the TRD results.

The two computational methods give equivalent results when dealing with the simulation of the unloaded GTEM cell, i.e., without the exposed biological sample. Although the TLM time domain algorithm requires higher computational resources than the analytical TRD one, it becomes advantageous for the simulation of the loaded GTEM cell which is no longer straightforward by the TRD method. In fact, the TRD method can calculate only the electromagnetic field pertaining to the unloaded GTEM cell, whereas the electromagnetic field inside the sample, indispensable to evaluate the SAR, must be calculated by a supplementary simulation with the Method of Moments (MoM) [1]. In particular, the MoM allows to evaluate the internal electromagnetic field from the incident one obtained by the TRD simulation.

Being the TLM a fullwave algorithm, it can simulate the GTEM cell and the exposed biological sample at once. Moreover, the numerical results presented in this paper have been obtained by using numerical parameters able to minimize the computational time and to reach a good agreement with the measurement results. In particular, the total number of elementary HSCN nodes used to simulate the whole GTEM cell is 183800, whereas the number of time steps is equal to 1000. These parameters lead to an acceptable computational time of about ten minutes on a computer with processor Intel Core i5 540 M–2.53 GHz and 4 GB of RAM.

Figure 4 shows the contour lines of the electric field components E_x (a), E_y (b), and E_z (c), calculated by the TLM algorithm, in the section $z = 0.230$ m. More precisely, the contour lines of Fig. 4 refer to the E-field components at frequency $f = 1.8$ GHz, for an input power $P_0 = 1$ W, and calculated at section $z = 0.230$ m in the case of unloaded GTEM cell (i.e., absence of the biological sample). Fig. 4 clearly highlights that, as it is expected in the case of TEM mode propagation, the e.m. field component E_y is dominant. In addition, Fig. 5 shows the electric field modulus $|E|$ calculated by the TLM algorithm in the section $z = 0.230$ m at frequency $f = 1.8$ GHz.

Owing to the tapered shape of the GTEM cell, some higher order modes are expected to propagate when the GTEM-cell cross section becomes large with respect to the wavelength. The propagation of higher order modes, due to the geometrical size of the GTEM cell, can be responsible for a perturbation of the e.m. field distribution with consequent non-uniformity of the dosimetric exposure. The amplitude of higher-order modes increases with the distance from the section in which they are excited [24]. Nonetheless, their contribution to the total e.m. field can be minimized by appropriately positioning the biological sample.

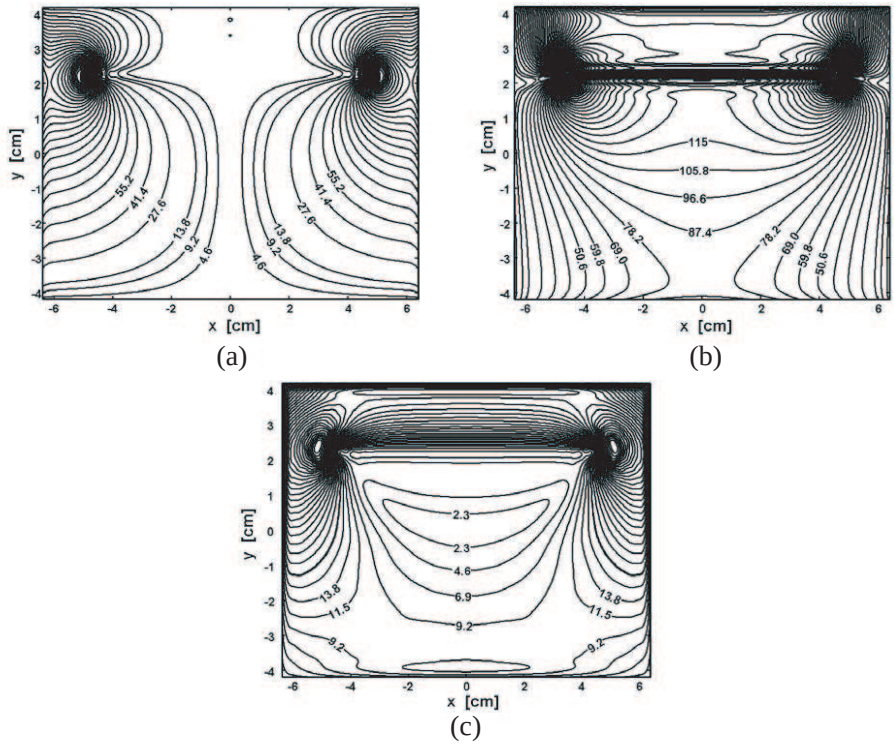

Figure 4. Electric field contour lines of the TEM mode. (a) E_x component [V/m]. (b) E_y component [V/m]. (c) E_z component [V/m] at $z = 0.230\,\text{m}$ and $f = 1.8\,\text{GHz}$.

The TLM does not involve the modal analysis of the GTEM cell, it being a full-wave technique and the overall calculated e.m. field resulting from the superimposition of all the propagating modes. Nonetheless, the propagation of TE and TM higher order modes can be qualitatively identified since those modes, differently from the dominant TEM mode, are characterized by non-negligible H_z and E_z components along the propagation direction.

Figure 4 clearly depicts that, in the case of unloaded GTEM cell, the E_z electric field component is averagely 20 times lower than the dominant E_y one, whereas E_z is 10 times lower than E_x. The same behavior was verified for the H_z magnetic field component. Since the ratio between the electromagnetic field components holds almost unchanged along the whole GTEM cell, the propagation of higher order modes practically does not influence the overall e.m. distribution, thus

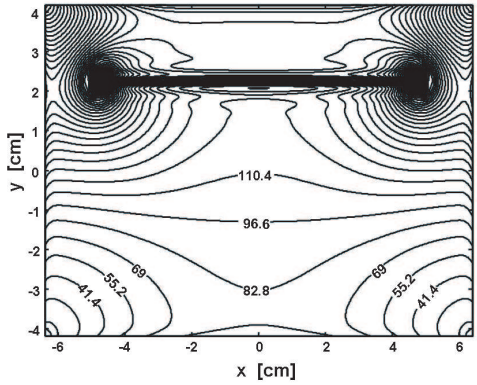

Figure 5. Electric field modulus $|E|$ [V/m] contour lines of the TEM mode at $z = 0.230\,\mathrm{m}$ and $f = 1.8\,\mathrm{GHz}$.

rendering the whole GTEM cell suitable for the dosimetric exposure tests. However, according to [25], the exposed sample height (h_s) must not exceed one third of the distance between the septum and the lower GTEM cell wall. This requirement implies that the optimal position for the biological sample, in our case of sample height $h_s = 0.020\,\mathrm{m}$, is $D = 0.230\,\mathrm{m}$.

It is worth mentioning that the aforesaid considerations refer to the incident e.m. field, i.e., in absence of the sample. Obviously, the insertion of the biological sample in the GTEM cell strongly perturbs the e.m. field according to the geometrical and dielectric characteristics of the sample. However, the optimal test region within the GTEM cell was defined taking into account the only incident wave. This approach gives useful information regardless of the dielectric and geometric characteristics of the biological sample specifically used in the experiment, provided a subsequent validation of this assumption by means of the SAR analysis.

3.1. Biological Sample Simulations

Aiming at the evaluation of the e.m. behavior of the GTEM cell, the exposure conditions pertaining to a cell medium sample were simulated by the TLM algorithm. The biological sample, inserted in the GTEM cell, was modeled by a cylinder having diameter $d_s = 0.040\,\mathrm{m}$ and height $h_s = 0.020\,\mathrm{m}$. The complex permittivity of the cell-medium was measured by using a coaxial probe setup (Agilent Technologies 85070C). The physical parameters of the exposed sample, relevant to the numerical e.m. simulation, are: density $\rho = 1000\,\mathrm{kg/m^3}$, measured

real part of the complex permittivity $\varepsilon_r = 77.1$, and measured conductivity $\sigma = 0.23\,\mathrm{S/m}$ at the frequency $f = 1.8\,\mathrm{GHz}$.

To reduce the numerical model complexity and the consequent computation time, the Petri dish plastic parts were neglected. Furthermore, a perfectly matched load was considered at the terminal section of the GTEM cell to avoid the supplementary simulation of absorbing materials.

Although simplified, the TLM numerical model proved effective in the e.m. and dosimetric characterizations of the GTEM cell exposure system in the sense that the obtained results are in good agreement with the ones obtained by the measurement as discussed in the following.

The main aim of this numerical model is to give the reference values of the SAR necessary to calibrate the experimental setup, i.e., to relate the SAR to the required input power. As described in the following, the numerical model is validated by comparison with the temperature measurement made on the reference medium, a 9-g/l saline solution. Once the numerical code has been validated, the exposure of different biological tissues can be safely predicted only by the TLM simulation, considering the complex permittivity of the new sample to be exposed. In particular, since the GTEM cell exposure setup is intended to be a ready-to-use system for the medical personnel involved in bioelectromagnetic experiments, with this approach, we aim to simplify the assessment of the dosimetric exposure. For this purpose, the TLM simulation program can be included in the user-friendly software which drives the experiment to preliminarily calculate the SAR and, therefore, to automatically set the required exposure parameters.

As an example, Fig. 6 shows the contour lines of E_x (a), E_y (b), and E_z (c) electric field components at frequency $f = 1.8\,\mathrm{GHz}$ in the $z = 0.230\,\mathrm{m}$ section, when the biological sample is inserted in the GTEM cell and centered at $D = 0.230\,\mathrm{m}$. The curves of Fig. 6 refer to an input power $P_0 = 1\,\mathrm{W}$ whereas the grey shaded rectangle denotes the sample area. For the sake of completeness, Fig. 7 shows the electric field modulus |E|calculated by the TLM algorithm in the section $z = 0.230\,\mathrm{m}$ at frequency $f = 1.8\,\mathrm{GHz}$, in presence of the sample.

The fullwave TLM simulation of the loaded GTEM cell, i.e., with the biological sample inserted, allows to take into account the perturbation of the electromagnetic field induced by the dielectric biological medium. In fact, the wave propagating in the loaded GTEM cell differs from the TEM mode pertaining to the unloaded GTEM cell, especially in the sample region. In fact, owing to the Faraday law,

the magnetic field components of the impinging TEM wave induce in the biological sample a not negligible electric field component E_z parallel to the propagation direction [26]. In addition, the overall e.m. field distribution within the sample can suffer from local spatial non-uniformity due to the wave reflections occurring at the sample-air interfaces. All these phenomena are taken into account by the full wave TLM simulation which allows the evaluation of the electric field inside the biological sample and, consequently, the calculation of the SAR.

By comparing Figs. 4 and 6, we point out the perturbation of the e.m. field pattern induced by the insertion of the biological sample. It is worth noticing that, as expected in this case, the E_z component is no longer negligible, thus the actual electromagnetic field within the sample differs from the TEM distribution.

The SAR distribution within the biological sample must be

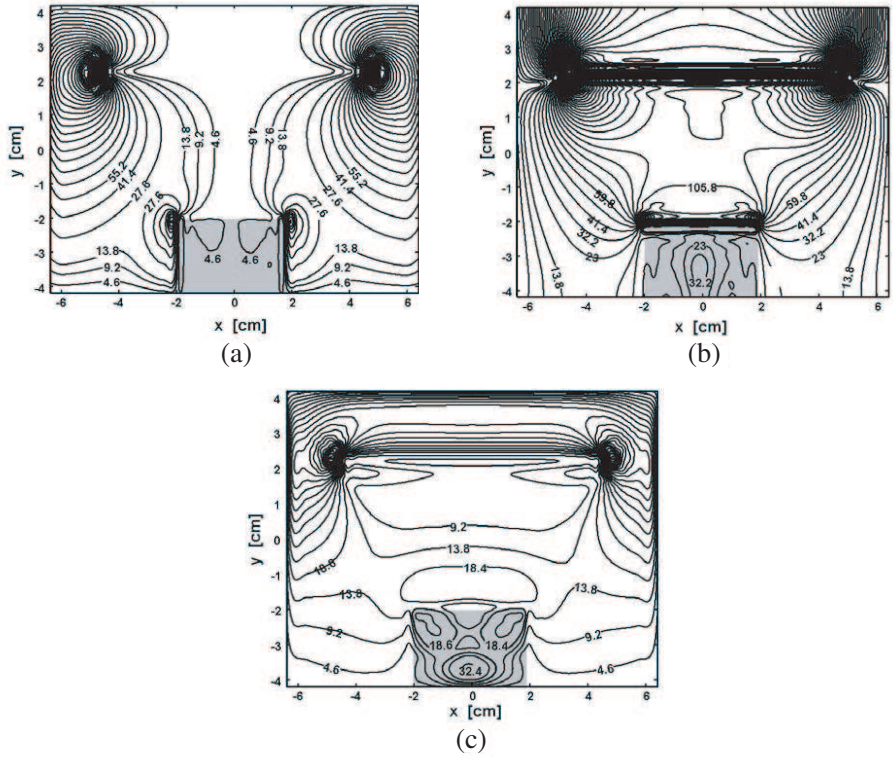

Figure 6. Electric field contour lines. (a) E_x component [V/m]. (b) E_y component [V/m]. (c) E_z component [V/m] at $z = 0.230\,\mathrm{m}$ and $f = 1.8\,\mathrm{GHz}$ with the inserted biological sample.

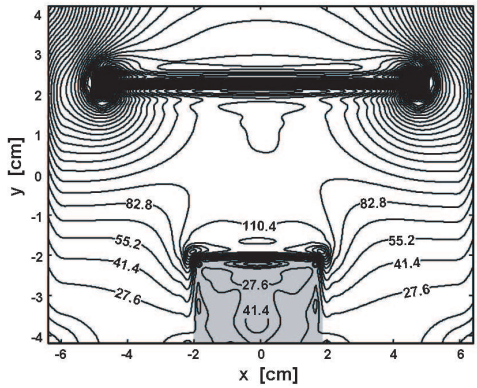

Figure 7. Electric field modulus $|E|$ [V/m] contour lines at $z = 0.230\,\mathrm{m}$ and $f = 1.8\,\mathrm{GHz}$ with the inserted biological sample.

carefully evaluated in order to guarantee the assessment of controllable and repeatable exposure conditions that can be easily linked to the possible biological effects induced by the e.m. exposure. For this aim, the local SAR of the biological sample was calculated by TLM simulations as it follows:

$$\mathrm{SAR}\,(i,j,k) = \frac{\sigma\,(i,j,k)\,|\mathbf{E}\,(i,j,k)|^2}{2\rho\,(i,j,k)} \tag{1}$$

In Eq. (1), $|\mathbf{E}\,(i,j,k)|$ is the internal electric field modulus, $\rho(i,\,j,\,k)$ is the mass density and $\sigma(i,\,j,\,k)$ is the conductivity of the biological sample expressed as a function of the position $(i,\,j,\,k)$ in the discretized space.

As a part of the validation, the results obtained by the TLM simulations were compared with those reported in [27]. In both cases, a whole blood sample, resembled by a parallelepiped having sizes $0.020\,\mathrm{m} \times 0.020\,\mathrm{m} \times 0.010\,\mathrm{m}$, relative permittivity $\varepsilon_r = 55.5$ and conductivity $\sigma = 1.86\,\mathrm{S/m}$, was simulated by considering an incident TEM wave with 224-$\mathrm{mW/m^2}$ power density at the frequency $f = 837\,\mathrm{MHz}$. Fig. 8 shows the SAR values calculated along a longitudinal line, parallel to the sample bottom and centered ($x' = 0$) within the biological sample at the height $y' = 0.005\,\mathrm{m}$. In particular, the results reported in [27] (triangles) and the corresponding fitting curve (dashed curve) were calculated by means of a high resolution FDTD (Finite Difference Time Domain) code. In this case a culture dish, fully filled with blood sample, was simulated centered on the septum of a TEM cell exposure system. Conversely, the TLM simulation results (dots in

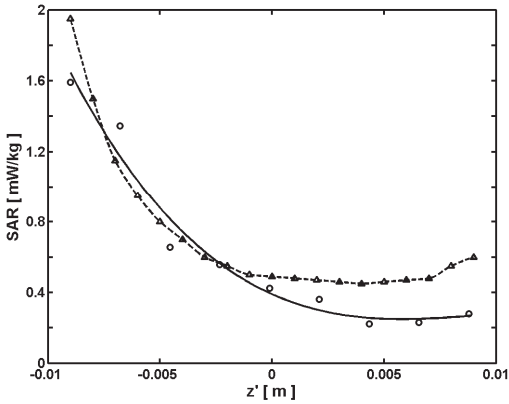

Figure 8. SAR of a blood sample along a longitudinal line centered at height $y' = 0.005\,\mathrm{m}$: Values calculated by FDTD [27] (triangles) and corresponding polynomial fitting curve (dashed line), values simulated by the TLM code (dots) and corresponding polynomial fitting curve (solid line).

Fig. 8) and the corresponding polynomial fitting curve (solid line) refer to the same blood sample exposed in the GTEM cell. Although two different exposure systems were considered, the aforesaid results are in good agreement since comparable exposure conditions pertain to the two different TEM waveguides.

In order to assess the exposure conditions achievable in the GTEM cell, the SAR of the cylindrical biological sample was evaluated in different positions D along the longitudinal direction parallel to the lower GTEM cell wall, as shown in Fig. 3. A cell medium sample, centered at the symmetry plane $x = 0\,\mathrm{m}$, was placed at different rise distances ($H = 0\,\mathrm{m}$, $H = 0.010\,\mathrm{m}$, and $H = 0.020\,\mathrm{m}$) from the lower GTEM cell wall. Fig. 9 shows the mean SAR, SAR_m, and the standard deviation σ_{SAR}, calculated within the overall sample volume, as a function of the sample position D. In particular, the circles of Fig. 9 refer to the simulated SAR_m values, the solid line refers to the corresponding polynomial fitting curve, whereas the dashed lines represent the standard deviation σ_{SAR} with respect to the mean SAR. Figs. 9(a), (b), and (c) refer to $H = 0\,\mathrm{m}$, $H = 0.010\,\mathrm{m}$, and $H = 0.020\,\mathrm{m}$, respectively. All reported values are evaluated by considering the input power $P_0 = 1\,\mathrm{W}$ and are averaged over the overall biological sample volume (diameter $d_s = 0.040\,\mathrm{m}$ and height $h_s = 0.020\,\mathrm{m}$). Fig. 9 shows that the SAR_m decreases with the distance from the input port owing to the reduced power density pertaining to

the larger sections of the tapered GTEM cell shape.

It is worth mentioning that, the obtained SAR values are affected by spatial non-uniformity, i.e., standard deviation σ_{SAR} averagely corresponds to 60%, 55% and 50% of the mean SAR for the three considered cases $H = 0\,\mathrm{m}$, $H = 0.010\,\mathrm{m}$, and $H = 0.020\,\mathrm{m}$, respectively. This behavior is mainly due to the numerical approach of the TLM model. In fact, the coarse staircase approximation (with HSCN elementary volumes equal to $8\,\mathrm{mm}^3$, corresponding to a total number of elementary volumes in the sample equal to 2480 which are all used to calculate the SAR standard deviation) of the GTEM-cell tapered shape and of the sample cylindrical geometry tends to increase the spatial fluctuation of the calculated e.m. field components. However, the optimization of the TLM numerical code, to enhance the numerical SAR uniformity for the exposure of single and multiple Petri dishes, is beyond the aims of this paper. Here, we wish to focus on the GTEM cell characterization by means of a numerical model that, although simple, can still effectively approximate the experimental conditions with moderate requirement of computational resources.

Nonetheless, the actual SAR inhomogeneity, apart from numerical inaccuracies, is expected to be higher for cell suspension (i.e., the exposed cells are floating in the whole culture medium) than for monolayers (i.e., the exposed cells are grown on the bottom surface of the Petri dish) [2]. Since higher inhomogeneity pertains to the SAR evaluated near the Petri dish walls, where the medium-air discontinuity occurs, the uniformity of SAR can be enhanced either by discarding the cells located at the sample edges or by including the Petri dish into a larger one filled with biological medium.

Figure 10 shows the SAR calculated in the plane $y' = 0.010\,\mathrm{m}$ at frequency $f = 1.8\,\mathrm{GHz}$, for a cell-medium sample placed at $z = 0.230\,\mathrm{m}$ from the pyramidal shape apex. The SAR distribution shown in Fig. 10 is referred to a local coordinate axes (x', and z') of Fig. 3. As expected, higher SAR values are found near the incidence plane at $z' = -0.020\,\mathrm{cm}$ whereas the mean and the standard deviation of the SAR are $\mathrm{SAR}_m = 1.13\,\mathrm{W/kg}$ and $\sigma_{\mathrm{SAR}} = 0.69\,\mathrm{W/kg}$, respectively, for an input power $P_0 = 1\,\mathrm{W}$. Thanks to the linear dependence of the SAR value with the input power, different exposure conditions can be easily assessed by properly varying the input power value.

It is worth considering that the e.m. power absorption induces a temperature increase in the biological sample. This effect must be properly controlled during the dosimetric experiments and eventually compensated in order to guarantee the optimal thermodynamic conditions necessary for the survival of the in vitro cultures (i.e., temperature $37^{\circ}\mathrm{C} \pm 0.1^{\circ}\mathrm{C}$).

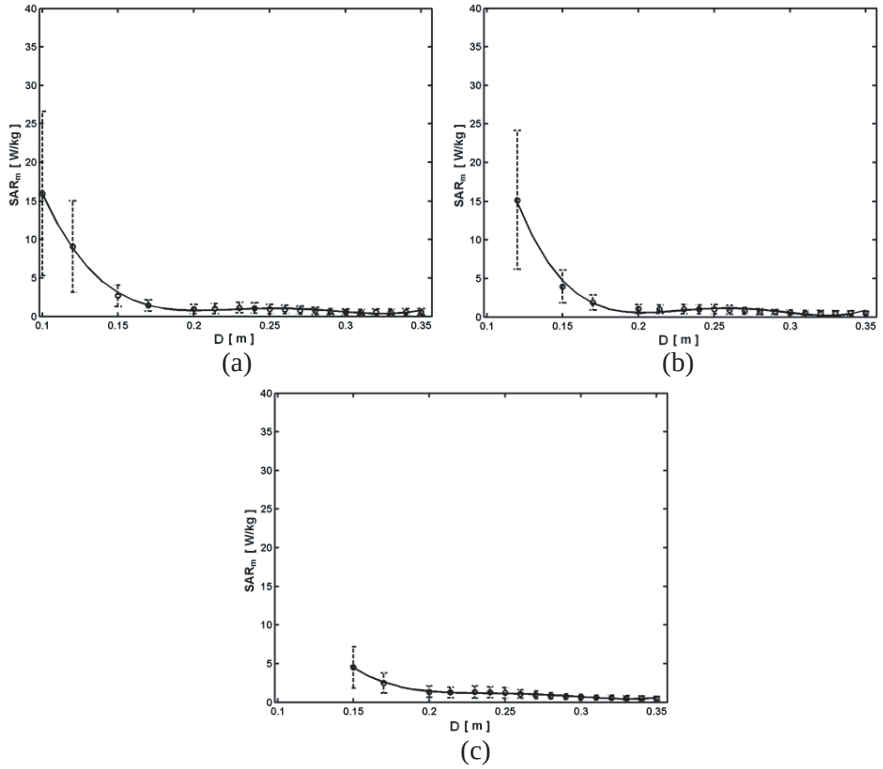

Figure 9. Simulated mean SAR values SAR_m (dots) and polynomial fitting curve (solid curve) as a function of the sample position D for different heights. (a) $H = 0\,\mathrm{m}$. (b) $H = 0.010\,\mathrm{m}$. (c) $H = 0.020\,\mathrm{m}$. The dashed lines correspond to the standard deviation of the SAR.

4. THERMAL SIMULATIONS OF THE EXPOSED BIOLOGICAL SAMPLE

The temperature increase induced in the biological sample by the absorbed e.m. power was numerically evaluated by means of the heat transfer equation [14, 22]:

$$\frac{\partial T\,(x,y,z,t)}{\partial t} = \alpha\ \nabla^2 T\,(x,y,z,t) + \frac{Q}{\rho\, c} \tag{2}$$

In Eq. (2) T is the temperature, α is the thermal diffusivity, c is the specific heat and ρ is the mass density. The heat source term $Q = \rho$ SAR is linked, by the mass density ρ of the biological medium, to the SAR calculated by the TLM method.

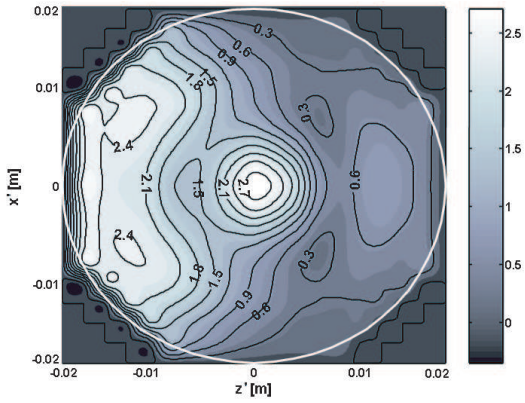

Figure 10. SAR calculated at plane $y' = 0.01\,\mathrm{m}$ from the Petri dish bottom and at frequency $f = 1.8\,\mathrm{GHz}$, for a cell-medium sample placed at $D = 0.230\,\mathrm{m}$.

Equation (2) has been solved by the FDTD algorithm. The heat transfer equation has been, therefore, discretized in the following explicit form:

$$T_{n+1} = \frac{\alpha\delta t}{\delta l^2}\left[T_n(i-1,j,k)+T_n(i+1,j,k)+T_n(i,j-1,k)+T_n(i,j+1,k)\right.$$
$$\left.+T_n(i,j,k-1)+T_n(i,j,k+1)\right]+\left(1-6\frac{\alpha\delta t}{\delta l^2}\right)T_n(i,j,k)+\frac{Q\delta t}{\rho c} \quad (3)$$

where the subscript n refers to the n-th discrete time interval δt and the indices i, j, k refer to the position in the discretized space (δl is the side size of each elementary cube that coincides with the TLM one $\delta l = \Delta l = 0.002\,\mathrm{m}$).

Convective boundary conditions

$$\kappa\frac{\partial T(x,y,z,t)}{\partial n} = h\left[T(x,y,z,t) - T_a\right] \quad (4)$$

have been considered at the biological sample interfaces. In Eq. (4), κ is the thermal conductivity, h is the heat transfer coefficient, and T_a is the temperature of the fluid surrounding the biological sample. The thermal parameters pertaining to the simulated biological sample are: specific heat capacity $c = 4187\,\mathrm{J(kgK)}^{-1}$, thermal conductivity $\kappa = 0.6\,\mathrm{W(Km)}^{-1}$ [2], and heat transfer coefficient $h = 10\,\mathrm{W(Km^2)}^{-1}$.

Equation (4) leads to the following FDTD discretized equation for the boundary elementary volumes:

$$T_{n+1}(i,j,k) = T_n(i,j,k) + \frac{h}{c\,\rho}\frac{\delta t}{\delta l}\left[T_a - T_n(i,j,k)\right].$$

The numerical stability of the FDTD algorithm is assured when [22].

$$\delta t < \frac{\delta x^2}{6\,\frac{\kappa}{c\rho}\left(1+\frac{h\,\delta x}{\kappa}\right)}.$$

It is worth mentioning that the electromagnetic and thermal phenomena evolve with different velocity. Therefore, the two physical phenomena were numerically evaluated by means of subsequent simulations, the time steps of which are significantly different ($\Delta t = 3.3\,\text{ps}$ and $\delta t = 1\,\text{s}$ for the electromagnetic and the thermal simulations, respectively).

As a part of the validation, the results of thermal simulations were compared with those obtained by the temperature measurements. According to the setup in Fig. 2, the temperature increase, induced in the biological sample by the e.m. irradiation, was measured by the optical temperature control probe (Luxtron m3300) during consecutive power-on and power-off time intervals. Fig. 11 compares the measured temperature increase ΔT (dots) with the corresponding simulated one (solid curve) obtained for SAR$= 1\,\text{W/kg}$ and initial temperature $T_{\text{ini}} = 37.0^{\circ}\text{C}$ at $x' = 0\,\text{m}$, $y' = 0.010\,\text{m}$, $z' = 0\,\text{m}$. Specifically, an initial power-off interval $t_{\text{ini}} = 900\,\text{s}$, useful to verify the thermal equilibrium within the GTEM cell, a power-on interval $t_{\text{on}} = 1800\,\text{s}$ and a following power-off interval $t_{\text{off}} = 2400\,\text{s}$ were considered. A good agreement between simulated and measured results is apparent.

By the agreement between the simulated and the measured temperature increase we can say that, although simplified, the TLM-FDTD model is able to predict the exposure conditions during the bioelectromagnetic experiments and that it can be used to calibrate the exposure setup, i.e., to choose the input power given the desired mean SAR value.

The temperature measurements can be also exploited to evaluate the SAR of the exposed sample according to the following equation, rigorous in the absence of thermal conduction and convection phenomena [2]:

$$\text{SAR} = c\frac{\Delta T}{\Delta t} \tag{5}$$

where c is the specific heat of the exposed medium, equal to $4187\,\text{J(kgK)}^{-1}$ for the saline solution. By Eq. (5), we evaluated the temperature increase in six different measurement points, casually chosen within the volume of the exposed sample (i.e., 9-g/l saline solution) placed at $D = 0.230\,\text{m}$. In particular, in each measurement point we obtained the temperature increase curves, similar to the one shown in Fig. 11, and we calculated, by Eq. (5), the SAR corresponding

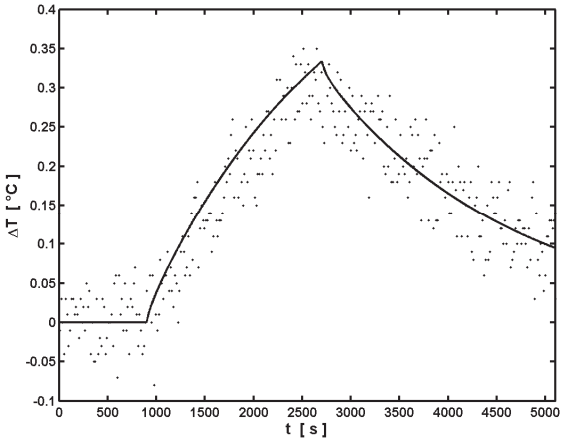

Figure 11. Biological sample temperature increase ΔT at $x' = 0\,\mathrm{m}$, $y' = 0.010\,\mathrm{m}$, and $z' = 0\,\mathrm{m}$, as a function of time: measured (dots) and simulated (solid curve) values.

to the initial slope of the measured data. The initial slope of the curves was used to minimize the influence of the thermal conduction and convection, since these phenomena become significant for longer observations of the temperature evolution with time. From the six measurement points we evaluated a mean SAR value $\mathrm{SAR}_m \approx 1\,\mathrm{W/kg}$ and a standard deviation σ_{SAR} of about 30%. This preliminary evaluation of the measured SAR uniformity seems to optimistically improve the numerical estimation of the SAR inhomogeneity. However, a more precise measurement of the SAR would require much more measurement points to strengthen the statistical analysis. This precise SAR evaluation is, however, beyond the aim of this paper and will be the object of a dedicated future work.

From the temperature measurement shown in Fig. 11 we can also infer that, for relatively high values of the average SAR (e.g., $\mathrm{SAR}_m = 1\,\mathrm{W/kg}$), the local temperature increase rapidly exceeds the maximum value $\Delta T = 0.1^{\circ}\mathrm{C}$ sustainable by the exposed cell culture.

The exposure setup must be capable of guaranteeing the temperature stability by using a proper cooling system (e.g., air or water cooling systems or Peltier cells) according to the particular exposure protocol to be performed. In fact, according to the specific biological effect to be investigated, the required exposure conditions can strongly differ as it concerns the SAR value and the exposure time. As an example, to parity of SAR value, a different effect could be induced by long-term exposure or by iterated short-term cycles

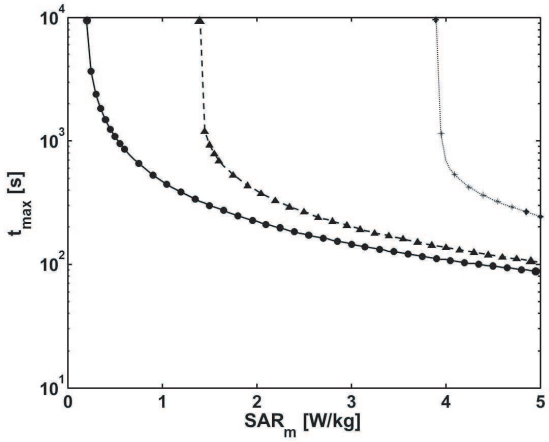

Figure 12. Maximum exposure time $t_{\max}$ corresponding to an average temperature increase $\Delta T_m = 0.1°\mathrm{C}$ within the sample as a function of the SAR_m for different equivalent heat transfer coefficients h: $h = 10\,\mathrm{W(Km^2)^{-1}}$ (dots and solid curve), $h = 100\,\mathrm{W(Km^2)^{-1}}$ (triangles and dashed curve), and $h = 1000\,\mathrm{W(Km^2)^{-1}}$ (asterisks and dotted curve).

of power-on and power-off intervals. Therefore, the dosimetric setup must allow different exposure conditions to be assessed in terms of SAR value and exposure time without exceeding the biological experiment constraints.

In order to establish the optimal exposure protocols, the temperature increase induced in the biological sample by the e.m. exposure was numerically evaluated by the TLM-FDTD code as a function of the mean SAR and of the exposure time. In particular, different cooling methods were simulated by considering an equivalent heat transfer coefficient h. This coefficient is typically $h = 10\,\mathrm{W(Km^2)^{-1}}$ in the case of free convection whereas it is typically $100\,\mathrm{W(Km^2)^{-1}}$ or $1000\,\mathrm{W(Km^2)^{-1}}$ in the case of forced convection of air or water, respectively [28, 29]. Fig. 12 shows the maximum exposure time $t_{\max}$ corresponding to the mean temperature increase $\Delta T_m = 0.1°\mathrm{C}$ as a function of the SAR_m, averaged in the overall sample volume. Specifically, the three curves of Fig. 12 refer to $h = 10\,\mathrm{W(Km^2)^{-1}}$ (solid curve), $h = 100\,\mathrm{W(Km^2)^{-1}}$ (dashed curve), and $h = 1000\,\mathrm{W(Km^2)^{-1}}$ (dotted curve). On the basis of calibration curves for the exposure duration of Fig. 12, the optimal protocol can be easily defined according to the requirements of the bioelectromagnetic experiment.

5. CONCLUSION

The electromagnetic and thermal analyses and characterization of a novel GTEM cell dosimetric setup for bioelectromagnetic experiments have been reported. The e.m. field distribution within the GTEM cell was evaluated in absence and in presence of the biological sample. Furthermore, the SAR distribution was evaluated as a function of the sample position. The optimal position for the biological sample was chosen at $D = 0.230\,\mathrm{m}$ from the input port where the average SAR is equal to $\mathrm{SAR}_m = 1.13 \pm 0.69\,\mathrm{W/kg}$.

In order to verify the temperature increase induced in the biological sample by the e.m. power absorption, the thermal analysis of the exposure system has been performed by applying the FDTD numerical method. A good agreement has been found between the simulated and the measured values of the temperature increase induced in the biological sample by the e.m. irradiation.

The novelty of the proposed system is mainly linked to its reduced sizes (0.45-m maximum length) with respect to the conventional GTEM cells, which are generally several meters long. Conventional GTEM cells have been successfully used to perform in vitro [9] and in vivo [10] experiments. However, these large-sized exposure systems are generally too expensive and space-demanding for medical laboratories devoted to the analysis of biological effects of e. m. fields. Moreover, they require a supplementary system for the control and the stabilization of the environmental conditions necessary for the survival of the exposed biological samples. The conventional GTEM cell, owing to its large sizes of a few meters, is also more expensive in terms of power required to achieve the desired exposure conditions. As an example, for a GTEM cell having $Z_0 = 50\,\Omega$ characteristic impedance and septum plate height $d = 1\,\mathrm{m}$, by roughly applying the well-known formula $E = \sqrt{P_{\mathrm{in}} Z_0}/d$ [18], an input power $P_{\mathrm{in}} = 200\,\mathrm{W}$ is required to issue an electric field $E = 100\,\mathrm{V/m}$.

The GTEM cell proposed in this paper overcome these drawbacks since, being only 0.45 m long, it can be inserted into a conventional incubator, typically used in medical laboratories, thus not requiring dedicated thermodynamic conditioning systems. The reduced sizes of the proposed GTEM cell are also advantageous since considerably lower values of input power are required to obtain the desired exposure conditions (i.e., input power $P_{\mathrm{in}} \approx 1\,\mathrm{W}$ to achieve an electric field $E = 100\,\mathrm{V/m}$ with septum plate height $d = 0.06\,\mathrm{m}$).

REFERENCES

1. Bozzetti, M., G. Calò, A. D'Orazio, M. De Sario, L. Mescia, V. Petruzzelli, and F. Prudenzano, "Optimized design of GTEM cells for dosimetric experiments," *Radio Science*, Vol. 42, RS3017, 2007.
2. Schuderer, J., T. Samaras, W. Oesch, D. Spät, and N. Kuster, "High peak SAR exposure unit with tight exposure and environmental control for in vitro experiments at 1800 MHz," *IEEE Trans. Microwave Theory Tech.*, Vol. 52, 2057–2066, 2004.
3. Laval, L., P. Leveque, and B. Jecko, "A new in vitro exposure device for the mobile frequency of 900 MHz," *Bioelectromagnetics*, Vol. 21, 255–263, 2000.
4. Merola, P., C. Marino, G. A. Lovisolo, R. Pinto, C. Laconi, and A. Negroni, "Proliferation and apoptosis in a neuroblastoma cell line exposed to 900 MHz modulated radiofrequency field," *Bioelectromagnetics*, Vol. 27, 164–171, 2006.
5. Balzano, Q., C. Chou, R. Cicchetti, A. Faraone, and R. Y.-S. Tay, "An efficient RF exposure system with precise whole-body average SAR determination for in vivo animal studies at 900 MHz," *IEEE Trans. Microwave Theory Tech.*, Vol. 48, No. 11, Part 2, 2040–2049, 2000.
6. Schonborn, F., K. Pokovic, and N. Kuster, "Dosimetric analysis of the carousel setup for the exposure of rats at 1.62 GHz," *Bioelectromagnetics*, Vol. 25, 16–26, 2004.
7. Biagi, P. F., L. Castellana, T. Maggipinto, G. Maggipinto, T. Ligonzo, L. Schiavulli, D. Loiacono, A. Ermini, M. Lasalvia, G. Perna, and V. Capozzi, "A reverberation chamber to investigate the possible effects of in vivo exposure of rats to 1.8 GHz electromagnetic fields: A preliminary study," *Progress In Electromagnetics Research*, Vol. 94, 133–152, 2009.
8. Zhen, J., C. Hagness, H. Booske, S. Mathur, and M. L. Meltz, "FDTD analysis of a gigahertz TEM cell for ultra-wideband pulse exposure studies of biological specimens," *IEEE Trans. Biomed. Eng.*, Vol. 53, No. 5, 780–789, 2006.
9. Zmyslony, M., P. Politanski, E. Rajkowska, W. Szymczak, and J. Jajte, "Acute exposure to 930 MHz CW electromagnetic radiation in vitro affects reactive oxygen species level in rat lymphocytes treated by iron ions," *Bioelectromagnetics*, Vol. 25, 324–328, 2004.
10. Bakos, J., G. Kubinyi, H. Sinay, and G. Thuroczy, "GSM modulated radiofrequency radiation does not affect

6-sulfatoxymelatonin excretion of rats," *Bioelectromagnetics*, Vol. 24, 531–534, 2003.

11. Liu, Y., Z. Liang, and Z.-Q. Yang, "Computation of electromagnetic dosimetry for human body using parallel FDTD algorithm combined with interpolation technique," *Progress In Electromagnetics Research*, Vol. 82, 95–107, 2008.
12. Zhang, M. and A. Alden, "Calculation of whole-body SAR from a 100 MHz dipole antenna," *Progress In Electromagnetics Research*, Vol. 119, 133–153, 2011.
13. Yanase, K. and A. Hirata, "Effective resistance of grounded humans for whole-body averaged SAR estimation at resonance frequencies," *Progress In Electromagnetics Research B*, Vol. 35, 15–27, 2011.
14. Taflove, A. and M. E. Brodwin, "Computation of the electromagnetic fields and induced temperatures within a model of the microwave-irradiated human eye," *IEEE Trans. Microwave Theory Tech.*, Vol. 23, No. 11, 888–896, 1975.
15. Mohsin, S. A., "Concentration of the specific absorption rate around deep brain stimulation electrodes during MRI," *Progress In Electromagnetics Research*, Vol. 121, 469–484, 2011.
16. Vita, A. De, R. P. Croce, I. M. Pinto, and B. Bisceglia, "Nonlinear interaction of electromagnetic radiation at the cell membrane level: Response to stochastic fields," *Progress In Electromagnetics Research B*, Vol. 33, 45–67, 2011.
17. Angulo, L. D., S. G. Garcia, M. F. Pantoja, C. C. Sanchez, and R. G. Martìn, "Improving the SAR distribution in petri-dish cell cultures," *Journal of Electromagnetic Waves and Applications*, Vol. 24, No. 5–6, 815–826, 2010.
18. Garbe, H. and D. Hansen, "The GTEM cell concept; applications of this new EMC test environment to radiated emission and susceptibility measurements," *Proc. 7th Int. Conf. Electromagnetic Compatibility*, 152–156, 1990.
19. Christopoulos, C., *The Transmission-Line Modelling Method TLM*, University of Nottingham, IEEE Press, New York, 1995.
20. Hang, J. and R. Vahldieck, "Direct derivations of TLM symmetrical condensed node and hybrid symmetrical condensed node from Maxwell's equations using centered differencing and averaging," *IEEE Trans. Microwave Theory Tech.*, Vol. 42, No. 12, 2554–2561, 1994.
21. Bozzetti, M., G. Calò, A. D'Orazio, V. Petruzzelli, F. Prudenzano, N. Diaferia, and C. Bonaventura, "Mode-stirred chamber for

cereal disinfestation," *Materials Research Innovations*, Vol. 8, 17–22, 2004.

22. Lizhuang, M., D. Paul, N. Pothecary, C. Railton, J. Bows, L. Barratt, J. Mullin, and D. Simons, "Experimental validation of a combined electromagnetic and thermal FDTD model of a microwave heating process," *IEEE Trans. Microwave Theory Tech.*, Vol. 43, 2565–2572, 1995.
23. Calò, G., F. Lattarulo, and V. Petruzzelli, "GTEM Cell experimental setup for in vitro dosimetry," *Journal of Communications Software and Systems*, Vol. 3, No. 1, 34–43, 2007.
24. De Leo, R., T. Rozzi, C. Svara, and L. Zappelli, "Rigorous analysis of the GTEM cell," *IEEE Trans. Microwave Theory Tech.*, Vol. 39, No. 3, 488–499, 1991.
25. IEC 61000-4-3, "Electromagnetic compatibility (EMC) testing and measurement techniques — Radiated, radio-frequency, electromagnetic field immunity test," 2003.
26. Pickard, W. F., W. L. Straube, and E. G. Moros, "Experimental and numerical determination of SAR distributions within culture flasks in a dielectric loaded radial transmission line," *IEEE Trans. Biomed. Eng.*, Vol. 47, No. 2, 202–208, Feb. 2000.
27. Lim, H. B., G. G. Cook, A. T. Barker, and L. A. Coulton, "FDTD design of RF dosimetry apparatus to quantify the effects of near fields from mobile handsets on stress response mechanisms of human whole blood," *Int. J. Numer. Model.*, Vol. 15, 563–577, 2002.
28. Holman, J. (ed.), *Heat Transfer*, 7th edition, McGraw-Hill, New York, 1990.
29. Incropera, F. P. and D. P. De Witt, *Introduction to Heat Transfer*, 2nd edition, John Wiley & Sons, New York, 1990.